JGR Space Physics

RESEARCH ARTICLE
10.1029/2024JA033464

D-Region Changes and Wave Activity Detected From Unusually Strong VLF Anomalies Associated With the January 2022 Tonga Volcanic Eruption

Sushil Kumar[1], **Sarwan Kumar**[1], **and Mie Ichihara**[2]

[1]School of Information Technology, Engineering, Mathematics and Physics (STEMP), The University of the South Pacific, Suva, Fiji, [2]Earthquake Research Institute, The University of Tokyo, Tokyo, Japan

Key Points:

- Unusually strong daytime signal amplitude anomalies of 11.1 dB on JJI and 12.6 dB on VTX signals recorded at Suva, Fiji
- Modeling using LWPC V2.1 showed a significant decrease in the D-region H' of 3.2 km and an increase in β of 0.319 km^{-1}
- Morlet wavelet analysis showed gravity waves of frequency 0.10–0.30 mHz responsible for VLF and D-region changes

Supporting Information:

Supporting Information may be found in the online version of this article.

Correspondence to:

S. Kumar,
sushil.kumar@usp.ac.fj

Citation:

Kumar, S., Kumar, S., & Ichihara, M. (2025). D-region changes and wave activity detected from unusually strong VLF anomalies associated with the January 2022 Tonga volcanic eruption. *Journal of Geophysical Research: Space Physics*, *130*, e2024JA033464. https://doi.org/10.1029/2024JA033464

Received 29 OCT 2024
Accepted 22 OCT 2025

Author Contributions:

Conceptualization: Sushil Kumar, Sarwan Kumar, Mie Ichihara
Data curation: Sarwan Kumar
Formal analysis: Sarwan Kumar
Investigation: Sushil Kumar, Mie Ichihara
Methodology: Sushil Kumar, Sarwan Kumar
Project administration: Sushil Kumar
Software: Sarwan Kumar
Validation: Sushil Kumar, Mie Ichihara
Visualization: Sushil Kumar
Writing – original draft: Sushil Kumar
Writing – review & editing: Sarwan Kumar, Mie Ichihara

Abstract We present unusually strong daytime signal amplitude anomalies of 11.1 dB on JJI and 12.6 dB on VTX very low-frequency (VLF) transmitter signals recorded at Suva, Fiji, due to the powerful Hunga Tonga–Hunga Ha'apai (HTHH) volcanic eruption (VE) on 15 January 2022 around 04:00 UT. Statistical analysis of daytime trends, daytime and nighttime fluctuations, and dispersion of VLF anomalies showed that VLF anomalies were indeed associated with HTHH VE. The combined effect of long-duration strong ionization produced by exceptionally intense volcanic lightning detected and Atmospheric Gravity Waves (AGWs) and Lamb Waves (LWs) associated with HTHH VE are reported here as causes of unusually strong VLF amplitude anomalies and D-region electron density changes. The daytime VLF anomalies extended into nighttime with reduced level that can be attributed to AGWs due to sustained HTHH volcanic lightning activity, as reported in the literature. Using the Long Wave Propagation Capability (code V2.1), we modeled VLF anomalies and found significant changes in the D-region VLF reference height (H') and electron density gradient (β). The H' for JJI path decreased significantly by 3.2 km, and β increased by 0.319 km^{-1}, giving an electron density increase from 1.83×10^2 cm^{-3} to 1.34×10^3 cm^{-3} at the normal daytime H' of 75.1 km. The perturbations in the D-region ionosphere are attributed to strong AGWs, mostly of frequency 0.10–0.30 mHz and LWs obtained using Morlet wavelet analysis of VLF anomalies, along with tremendously high lightning strokes demonstrating coupling between the atmosphere and the D-region.

Plain Language Summary The extraordinary underwater Hunga Tonga-Hunga Ha'apai (HTHH) volcanic eruption (VE) triggered global disturbances in the Earth's atmosphere, including the ionosphere. Ionospheric changes have been studied using several techniques such as Global Navigation Satellite System (total electron content), ionosonde, and airglow emission. The very low frequency (VLF) is a cost-effective radio wave technique that has been successfully used to study the lower ionospheric changes associated with extreme space weather (e.g., solar flares and geomagnetic storms) and terrestrial weather events (earthquakes, tropical cyclones, eruptive events). VLF (3–30 kHz) and low frequency (30–300 kHz) radio waves propagate by multiple reflections between a spherical waveguide between the Earth and the lower ionosphere (D-region) with a very low attenuation of 1–2 dB/1,000 km. They form a novel tool for diagnosing the D-region under normal and disturbed conditions. This is the first study to provide a holistic view of D-region changes due to HTHH VE, considering other severe space and terrestrial weather events.

1. Introduction

A powerful underwater volcanic eruption (VE) in Hunga Tonga–Hunga Ha'apai (HTHH) occurred at the geographic location (20.550°S, 175.385°W) on 15 January 2022 shortly after 04:00 UT (Astafyeva et al., 2022; Horiuchi et al., 2024; Vergoz et al., 2022) following the several weeks of activity. Analyses of the various observational data suggested multiple bursts in several hours (e.g., Astafyeva et al., 2022; Ichihara et al., 2023; Poli & Shapiro, 2022; Vergoz et al., 2022; Wright et al., 2022). Among them, Astafyeva et al. (2022), who analyzed ionospheric perturbation, reported that at least five major explosions occurred between ~04:08 and 08:20 UT. The estimated energy of the HTHH VE ranged from 4 to 200 Megatons of trinitrotoluene equivalent (Astafyeva et al., 2022; Kulichkov et al., 2022) and was strongest in the last 30 years (Duncombe, 2022). A wide spectrum of atmospheric waves, such as acoustic waves (AWs) and atmospheric gravity waves (AGWs), large amplitude Lamb waves (LWs), and tsunami waves, were associated with HTHH VE (e.g., Ghent & Crowell, 2022; Matoza et al., 2022; Wright et al., 2022). This explosion was heard thousands of km from the

eruption center, including by the article's lead author in Fiji, which appeared like a very strong thunderstorm that even shook the house windows due to the shock of high-frequency acoustic waves.

A commonly used parameter in volcanology is the Volcanic Explosivity Index (VEI), which is derived from the volumes of material ejected, the heights of ash columns, and the style and duration of the eruption (Newhall & Stephen, 1982). VEI has a scale from 0 to 8. While eruptions with a VEI of 0 occur continuously, those with a VEI of 8 are uncommon, occurring only once every 50,000 years (Astafyeva, 2019). HTHH submarine volcano exploded and produced the largest volcanic eruption of the modern era reaching a VEI of 5–6 (Poli & Shapiro, 2022; Vergoz et al., 2022; Yuen et al., 2022). Explosive eruptions from volcanoes eject material (rocks, ash, gas) up into the atmosphere and produce a wide spectrum of pressure waves that cause violent atmospheric displacements and can travel up to ionospheric heights where they induce fluctuations in the ionospheric electron density (Nakashima et al., 2016). The exceptional HTHH VE on 15 January 2022 produced a lot of interest in the ionospheric scientific community, and several ionospheric studies (e.g., Astafyeva et al., 2022; Li et al., 2023; Liu et al., 2023; Pradipta et al., 2023; Themens et al., 2022; Vadas et al., 2023; Zhang et al., 2022 and references therein) have been carried out using the GNSS-based observations at the local, regional, and global scales. However, a very small number of studies (Ohya et al., 2024; Solovieva & Shalimov, 2022; Solovieva et al., 2022) have been carried out on the very low frequency (VLF)/low frequency (LF) perturbations associated with HTHH VE, which is the subject of this paper.

Any sudden powerful blasts such as VEs, strong earthquakes, nuclear explosions and powerful rocket launches can potentially launch “internal” AWs and AGWs (e.g., Fritts & Alexander, 2003; Hines, 1960; Huang et al., 2019; Igarashi et al., 1994; Richmond, 1978). The AWs propagate isotropically outward and AGWs propagate obliquely outward from the explosive event location (Huang et al., 2019). As the AWs and AGWs propagate upward with exponentially increased amplitude with the height due to an exponential decrease in atmospheric density, they interact/couple with the ionospheric plasma (D, E, and F layers). They can generate traveling ionospheric disturbances (TIDs) (e.g., Huang et al., 2019). The D-region is a mixture of thin plasma and dense neutral atmosphere, resulting in high collision frequency between electrons and neutrals, as well as high recombination rates. It can quickly respond to geophysical phenomena, making it a natural laboratory for detecting earthquakes, VEs and tropical cyclones. In the D-region, VE associated perturbations can be detected in sub-ionospheric VLF/LF signals transmitted by navigational transmitters and strong lightning discharges which propagate to global distances by multiple reflections in the Earth-ionosphere waveguide with very low attenuation of 1–2 dB/1,000 km (Cummer et al., 1998; S. Kumar et al., 1994) and form a novel tool to diagnose lower ionosphere (D-region) and detect the atmospheric waves propagating through it (e.g., S. Kumar et al., 2017; Xu et al., 2024).

In this work, the sub-ionospheric JJI VLF transmitter signal (22.2 kHz), Japan (geog. location 32.05°N, 130.83°E), and VTX VLF transmitter signal (18.2 kHz), India (8.392°N, 77.75°E) received at a low latitude station, Suva (18.14°S, 178.44°E), Fiji, have been used to determine any daytime VLF anomaly/D-region changes and atmospheric wave activity in the D-region due to exceptionally intense HTHH VE on 15 January 2022. The daytime strong signal anomalies and D-region changes associated with HTHH VE have not been reported so far (to our knowledge). The Suva VLF station is located northwest of the HTHH eruption location (20.550°S, 175.385°W) at about 701 km. The transmitter-receiver great circle paths (TRGCPs) of the JJI and VTX signals to Suva, Fiji, and the location of the HTHH eruption are shown in Figure 1. The TRGCP distance is 7.5 Mm for the JJI signal and 11.12 Mm for the VTX signal.

2. Data and Analysis

Sub-ionospheric VLF signals from four mid-latitude transmitters, JG2AS, JJI, NAA, and NLK, and three low-latitude transmitters, NPM, NWC, and VTX, were recorded at Suva, Fiji, using the SoftPAL system (A. Kumar & Kumar, 2020). For this study, only JJI and VTX transmitter signals recorded from 7 to 23 January 2022 were used to avoid overlapping of volcanic eruption associated VLF perturbations with amplitude minima/fading associated with sunset transition over the station. VLF perturbations over these two transmitter signals occurred before the occurrence of solar terminator associated amplitude minima. The solar terminator passage (sunrise and sunset) generates the atmospheric AGWs, which can be detected in the D-region using the VLF radio wave technique (Nina & Čadež, 2013).

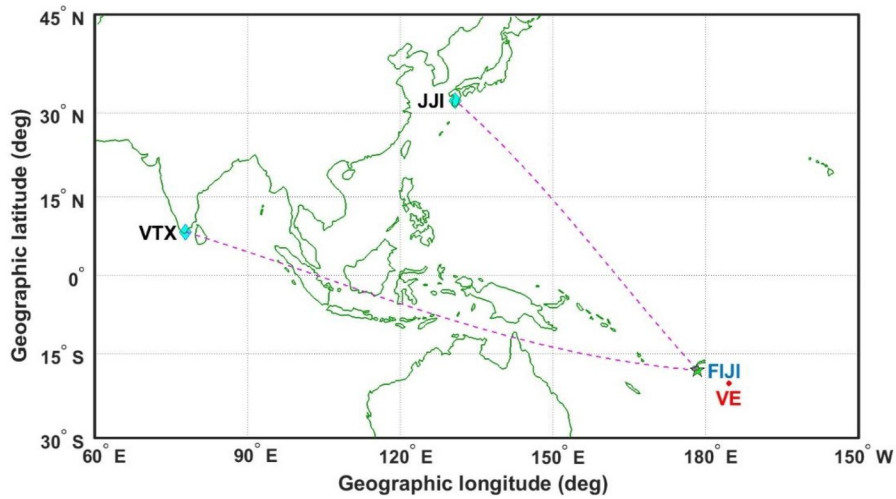

Figure 1. Relative location of the JJI and VTX transmitters (cyan diamond), receiver station Suva (green star), and their transmitter-receiver great circle paths (TRGCPs). The location of the Hunga Tonga–Hunga Ha'apai (HTHH) volcanic eruption epicenter (VE) is marked with a solid red circle.

For daytime and nighttime amplitude, we separately determined the statistical quantities such as trend, daytime and nighttime fluctuation (DF and NF) and dispersion (square root of the variance). Note that dispersion here is not the dispersion of the waves, rather is the standard deviation of the signal amplitude. The fluctuation in the daytime and nighttime average signal amplitude was obtained using:

$$dA(t) = A(t) - A_{av}(t) \tag{1}$$

where $dA(t)$ is the difference between the signal amplitude and the standard average at a particular time t. $A(t)$ is the VLF signal amplitude at a particular time t during the day or night, and $A_{av}(t)$ is the standard average amplitude over ±8 days at a particular time t. The trend is the average of $dA(t)$ values for each day and night. DF is the integral of $[dA(t)]^2$ values over the individual daytime hours. The NF is calculated in a similar way for individual nighttime hours. Dispersion (D) is the standard deviation of $dA(t)$ values for each day and night (Hayakawa et al., 2010).

The 1-min signal amplitude and phase values were used in this study. VE induced perturbations in the amplitude (ΔA) of these VLF signals were obtained using the procedure given by Todoroki et al. (2007);

$$\Delta A = A_{\text{peak}} - A_{\text{background}} \tag{2}$$

A_{peak} is the peak amplitude during a VE, and $A_{\text{background}}$ is the mean amplitude value of certain days from the month of VE occurrence at the same time intervals. VE induced perturbation in the phase ($\Delta\phi$), was determined from the phase difference between baseline and signal anomaly of same time and day.

Long Wave Propagation Capability (LWPC) code V2.1 has been utilized to determine HTHH VE associated changes in D-region parameters (Wait & Spies, 1964), which are the D-region VLF reference height (H') and electron density gradient (β) (rate of increase of electron density with height). The Wait-Spies model is not the most accurate representation of the D-region, but it best reproduces VLF propagation at a specific frequency and has been used in several VLF/LF remote sensing scientific investigations of the D-region (e.g., A. Kumar & Kumar, 2020; S. Kumar et al., 2017; Thomson et al., 2014, 2021). LWPC code is an assembly of separate and self-complete programs used to model the VLF signal propagation characteristics. The Space and Naval Warfare System Center in San Diego created this code, which uses an exponentially increasing conductivity with the height model of the D-region (Ferguson, 1998). A reader is referred to modeling works for further details of LWPC code applications to the D-region (e.g., A. Kumar & Kumar, 2020; S. Kumar et al., 2017, 2023; McRae & Thomson, 2000). First, we determined the normal signal amplitude A, H', and β during the unperturbed/normal condition (quiet period) using LWPC. From the VLF signal amplitude perturbation due to the HTHH eruption, we

calculated the ΔA using Equation 2. The measured ΔA and $\Delta\phi$ are added to the normal signal amplitude and phase (A and ϕ) obtained from LWPC (unperturbed condition) to find the perturbed signal amplitude and phase (A' and ϕ') due to a volcanic eruption. For the perturbed ionosphere, values of H' and β were obtained from the match between the LWPC generated amplitude and phase and A' and ϕ'. The LWPC modeling of perturbed signal amplitude and phase A' and ϕ' gives a unique value of path integrated H' and β, which produce the amplitude and phase values that match their disturbed values (A' and ϕ') at a distant receiver.

Moreover, Wait and Spies (1964) proposed a simple exponential lower ionosphere model consisting of two parameters, the H' and β, in the electron density $Ne(h)$ profile as a function of height h, given as:

$$Ne(h) = 1.43 \times 10^{7} [\exp(-0.15\, H') \exp(\beta - 0.15)(h - H')] \quad (3)$$

where H' and β are in km and km^{-1}, respectively. This equation is most commonly used by researchers such as S. Kumar et al. (2017) and Thomson et al. (2014) for $Ne(h)$ effective up to an altitude of 100 km.

We have applied the mother Morlet wavelet technique (Mallat, 1999) on the JJI and VTX VLF transmitters signal amplitude during 7–23 January to find if there are any wave-like signatures (WLS) present in the signal amplitude due to HTHH VE associated atmospheric waves. We obtained the wavelet spectra of amplitude perturbation of both signals by finding the amplitude difference between ±8 days' average from VE day (15 January 2022) for (a) 24 hr, and (b) daytime and (c) nighttime (dark) of TRGCPs. Since there were no solar flares of class C and above around the time of eruption occurrence to affect the D-region ionosphere, therefore, the wave-like signatures (WLS) seen in the wavelet spectra are considered due to HTHH VE.

3. Results

3.1. JJI to Suva Path: Volcanic Eruption on 15 January 2022

Figure 2a presents JJI VLF signal amplitude diurnal variation from 7 to 23 January, which includes the mean of 8 days (green line) prior, the mean of 8 days (blue line) after, and the HTHH VE day amplitude (red solid line, 15 January). It shows a clear enhancement of signal amplitude on VE day over the mean values of ±8 days, separately. A further check of the January 2021 VLF data (Figure S1a in Supporting Information S1) confirms that this strong signal enhancement was due to HTHH VE. Figure 2b shows the mean amplitude (black line) on geomagnetically quiet (Q) days of the month with ±2 standard deviation (σ) (gray line) and ±3σ (blue line), and VE day amplitude (red line). The excursion in the amplitude outside ±2σ and ±3σ (σ is the standard deviation) on 15 January indicates a VE associated enhancement in the amplitude, the peak of which is marked by VE (red font). For stronger confidence (>95%), perturbations exceeding 3σ are considered due to VE rather than day-to-day variability (S. Kumar et al., 2017). Figure 2c shows amplitude variation on a day prior (14 January) and a day after (16 January) the volcanic eruption day (15 January). The local time of Fiji is LT = UT + 12 hr. The periods corresponding to sunset, 6–9 UT (18–21 LT) and sunrise, 17–22 UT (5–10 LT) transitions, have been indicated between the gray shaded region. During VE day, for about 2 hr (04:28–06:24 UT) in the daylight of JJI-Suva TRGCP, the signal amplitude increased significantly with a maximum ΔA = 11.1 dB (Equation 2) from the Q days mean value at 4:58 UT before the sunset transition. The signal amplitude fluctuations also occurred during nighttime, above the mean values of ±8 days (Figure 2b), but were mostly within the ±3σ limits. The JJI VLF signal phase variation during 14–16 January 2022, which includes a day prior (14 January, green line) and a day after (16 January, blue line) the HTHH VE day (15 January, red line) was checked (Figure S2 in Supporting Information S1). Despite the phase being unstable (building continuously), a clear signature of an increase in phase was observed due to HTHH VE with a phase difference of 416.8° measured between the baseline (linear fit line) and the peak of the signal anomaly (Figure S2 in Supporting Information S1). Statistical analysis of the trend, fluctuation and dispersion (standard deviation) for daytime and nighttime of the signal amplitude was carried out to verify the perturbations caused by VE, where the signal anomaly is considered by the simultaneous drop/rise in the trend and rise in the fluctuation and dispersion (Hayakawa et al., 2010; S. Kumar et al., 2022). Figure 3 presents the graphical representation of the trend (a and d), fluctuation (b and e) and dispersion (c and f) in each panel for the JJI VLF signal amplitude during the period from 07–23 January 2022. The panels (a–c) on the left side represent daytime, while the panels (d–f) on the right side represent nighttime. The purple and blue horizontal dashed lines show the ±1σ and ±2σ criteria, respectively. The green bar represents the volcanic eruption day and the red circle on the bar indicates anomalous values on 15 January 2022 (values crossing the ±1σ and ±2σ lines)

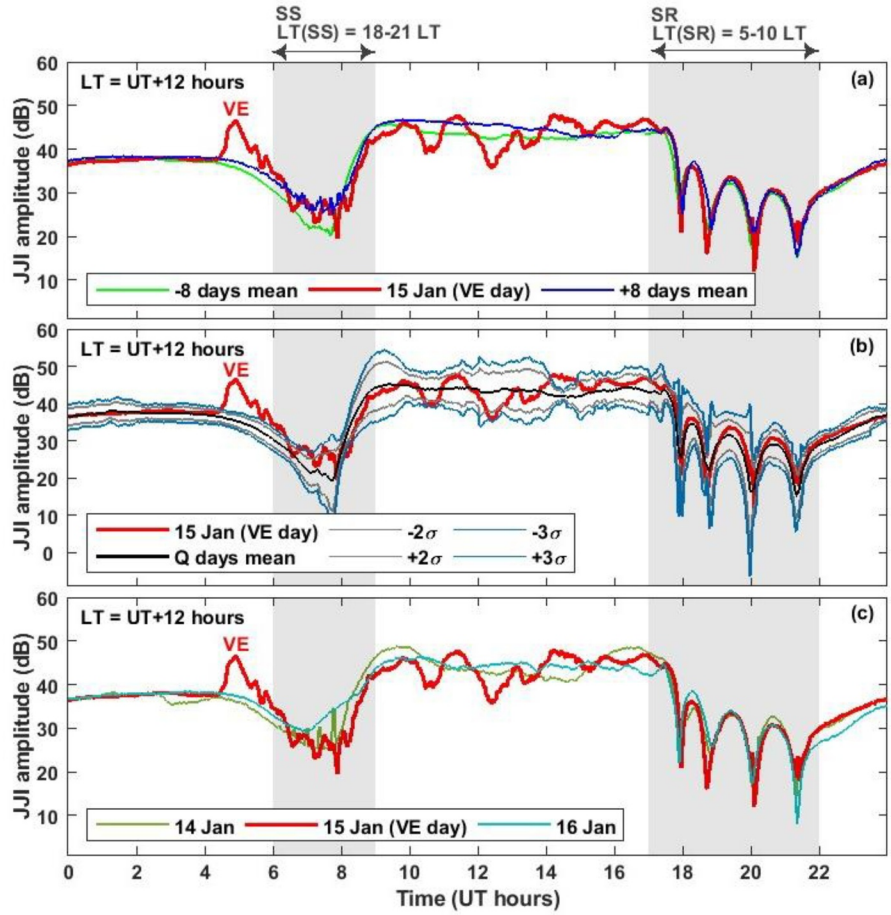

Figure 2. (a) JJI VLF signal amplitude variations against time (UT) during 7–23 January 2022 which includes 8 days prior (−8 days mean, green line) and 8 days after (+8 days mean, blue line) the volcanic eruption on 15 January 2022 (red line), (b) the geomagnetically quiet (Q) days mean amplitude (black line), ±2σ (gray line) and ±3σ (blue line) and (c) a day prior (14 January) and a day after (16 January) the volcanic eruption day (15 January). Excursion in the amplitude outside ±2σ and ±3σ on 15 January 2022 is marked as VE. The periods corresponding to sunset (SS) and sunrise (SR) transitions are indicated between the gray shaded region. LT = UT + 12 hr.

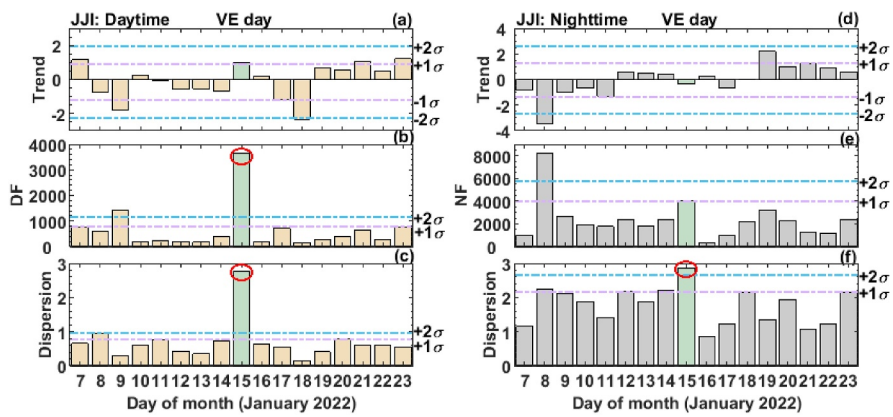

Figure 3. Graphical representation of the trend (a and d), fluctuation (b and e) and dispersion (c and f) in each panel for JJI VLF signal amplitude during the period from 7–23 January 2022. The panels (a–c) on the left side represent daytime while the panels (d–f) on the right side represent nighttime. The purple and blue horizontal dashed lines show the ±1σ and ±2σ criteria, respectively. The green bars represent the volcanic eruption day, and the red circle on the bar indicates anomalous values on 15 January 2022 (values crossing the ±1σ and ±2σ lines).

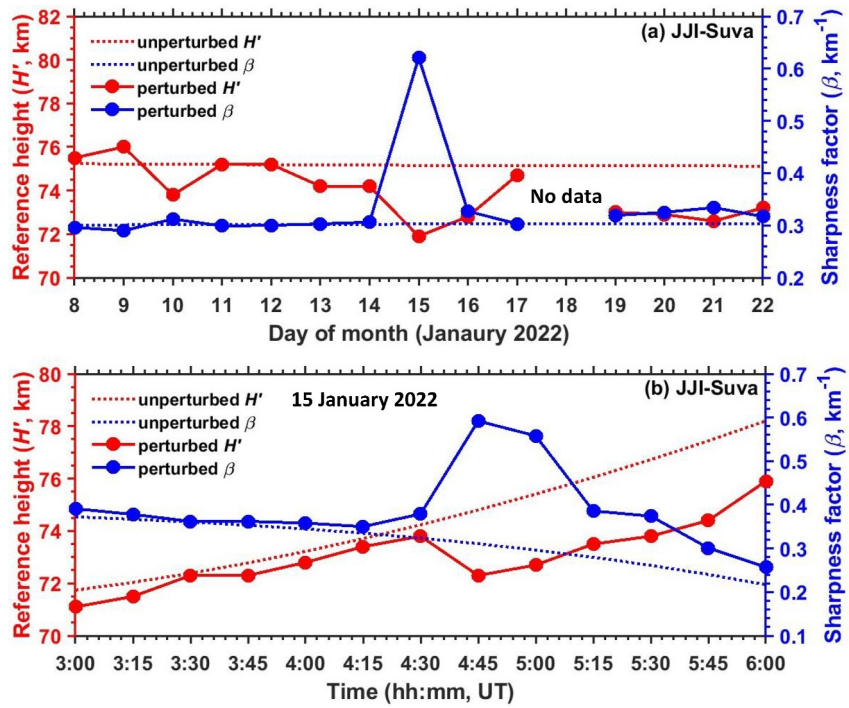

Figure 4. (a) Variation of the ionospheric Wait parameters: H' (red) and β (blue) associated with the daytime JJI signal to Suva every day at 4:54 UT from 8 to 22 January 2022 and (b) Temporal variation of the ionospheric Wait parameters associated with the daytime JJI signal to Suva for a period 3:00–6:00 UT (including signal anomaly) on 15 January 2022. The normal (unperturbed) values are shown by dashed lines. LT = UT + 12 hr.

due to the VE. For stronger confidence, we consider anomalies outside the ±2σ line on the VE day. The trend value does not touch the ±2σ line on the day of the VE (panel a and d). The daytime fluctuation crossed the +2σ line on the VE day (panel 3b) with an abnormally high increase. Similarly, the dispersion during daytime and nighttime on the VE day crossed the +2σ line (panels c and f), with daytime fluctuations higher than nighttime. Although nighttime fluctuations and dispersion were higher than normal values, a significantly higher difference compared with normal days was observed during the daytime due to an unusually high increase in the signal amplitude during 04:28–06:24 UT (16:28–18:24 LT).

The D-region perturbation is assumed to be uniform along the entire TRGCP under the pure day and night periods, and the LWPC code has been used to estimate the path-integrated (average) unperturbed and path-integrated perturbed Wait parameters H' and β for the daytime VLF perturbations (anomaly) associated with HTHH VE. Figure 4a shows the H' (red) and β (blue) variations every day at 4:54 UT from 8 to 22 January 2022. H' and β showed smooth variations before and after the HTHH VE day of 15 January, on which H' decreased and β increased sharply during the signal anomaly period. The H' and β variation for about an hour before and after the HTHH VE (03:00–06:00 UT) at every 15 min duration is shown in Figure 4b. The H' increased progressively from 03:00 UT until the signal anomaly due to daytime progressing toward night and then decreased during the signal anomaly during which β increased sharply. During the VE day, from LWPC modeling, path integrated (average) perturbed values of H' and β at the peak of signal amplitude anomaly were estimated to be 71.9 km and 0.621 km^{-1}, respectively, showing a decrease in H' by 3.2 km and an increase in β by 0.319 km^{-1} at 4:54 UT on 15 January from normal values of H' = 75.1 km and β = 0.302 km^{-1} obtained using the method proposed by McRae and Thomson (2000). Figure 5 presents the plot of electron density, $Ne(h)$, versus ionospheric height, where the electron density profile for the unperturbed and perturbed conditions are denoted as a black dashed line and red solid line, respectively. The height range was selected from 70 to 90 km, which covers the day and nighttime VLF reflection heights in the D-region. The electron density was significantly larger under HTHH VE conditions compared to normal conditions (Figure 5). The average path-integrated $Ne(h)$ from 1.83×10^2 cm^{-3} at daytime normal h = 75.1 km increased significantly to 1.34×10^3 cm^{-3}. As seen from the figure, the electron density under the disturbed conditions increased rapidly with height, which at a height of 90 km increased from

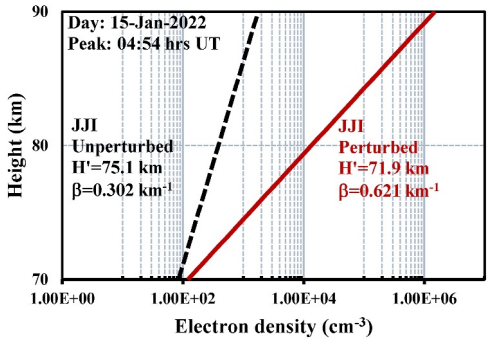

Figure 5. The perturbed electron density due to the HTHH volcanic eruption on 15 January 2022 with a peak at 04:54 UT for the JJI (red solid line) compared with the normal unperturbed electron density for the JJI (black dashed line) to Suva path in the altitude range of 70–90 km.

1.34×10^3 cm^{-3} to 1.46×10^6 cm^{-3}. This is partly due to the limitations of the Wait and Spies and LWPC models, because the former takes the same value of β for all altitudes, and the latter gives a β value at the disturbed height only.

Morlet wavelet analysis for the JII signal amplitude at Suva was carried out during 14–16 January 2022. The wavelet spectra were determined during 7–23 January 2022, since no signatures of wave activity were seen except during the HTHH VE. We finally selected 1 day before and after the VE day. Figure 6 presents the Morlet wavelet analysis for signatures of atmospheric AGWs in the low-frequency range (0.00–1.0 mHz) in the JJI signal amplitude perturbations. Panels a and b represent the wavelet spectra of signal amplitude for 24 hr (including terminator times sunset, SS and sunrise, SR) and excluding duration of SS and SR transitions which have daytime (DT, daylight) (00–06 UT or 12–18 LT) and nighttime (NT, dark) (09–17 UT or 21–05 LT) of the TRGCP, respectively, during 14–16 January 2022. In panel 6a, the stronger wave-like signatures (WLS) with frequencies ranging from 0.05 to 0.25 mHz are clearly revealed. The weaker WLS of 0.25–1 mHz are mostly limited to the duration of sunrise/sunset terminator transition times due to amplitude minima occurring during these times because of modal interferences. To avoid the effect of the terminator transition, shown in Figure 6b, the wavelet analysis was performed for pure daylight (6 hr per day) and night (8 hr per day) during 14–16 January 2022. Due to this time duration limitation, we have filtered any WLS component below 0.1 mHz (panel b) to obtain the true physical WLS signals. As shown in panel 6b, the WLS in the frequency range of 0.10–0.25 mHz and comparatively weaker WLS in the range of 0.25–0.35 mHz were observed during daytime on 15 January (VE day) and nighttime on 16 January. To look for higher frequency AGWs from 1.0 mHz to below 2.9 mHz and AWs $\geq$ 3.3 mHz, a wavelet analysis in the frequency range of 1–6 mHz is presented in Figure 7 for the same format of the data as in Figure 6, which shows weak WLS in the range of 1–3 mHz, almost no signatures of AGWs and normal AWs $\geq$ 3.3 mHz. The AGWs in the frequency range ~1–3 mHz (panel a) are of solar terminator origin, as they occurred during the solar terminator transition over the path.

3.2. VTX to Suva Path: Volcanic Eruption on 15 January 2022

Figure 8a shows the VTX VLF signal amplitude diurnal variation from 14 to 23 January, including the day before (green line), the mean of 8 days after (blue line) and the HTHH VE day amplitude (red solid line) on 15 January. Unlike JJI signal analysis, we could not show 8 days of data before the VE day because the transmitter was off-air from 7 to 13 January. Otherwise, the data format in Figures 8a–8c is the same as in Figures 2a–2c. During VE day, approximately for 1 hr (04:35–05:32 UT) in the daylight of VTX-Suva TRGCP, the signal amplitude increased with maximum ΔA = ~12.6 dB (Equation 2) from the Q-days mean value at 4:54 UT before the sunset transition,

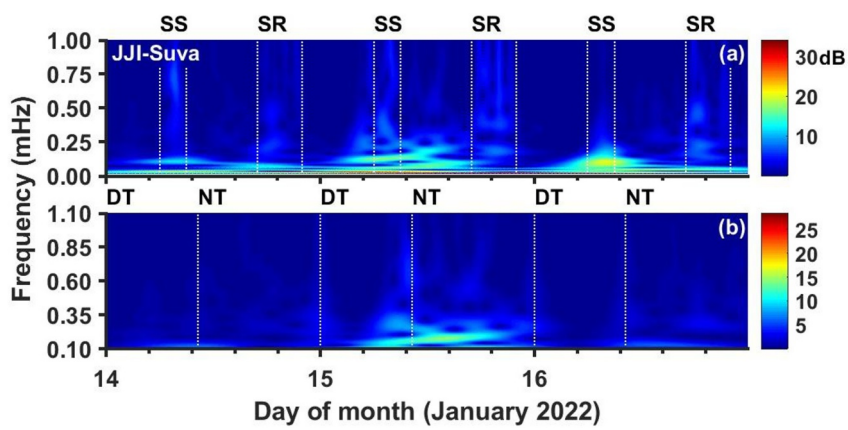

Figure 6. The wavelet spectra of JJI signal amplitude perturbations in the frequency range of 00–1.0 mHz presented in panels: (a) 24 hr (including terminator times marked as SS and SR) and (b) during daylight (DT, 00–06 UT) and night (NT, 09–17 UT) periods of the TRGCP from 14 to 16 January 2022.

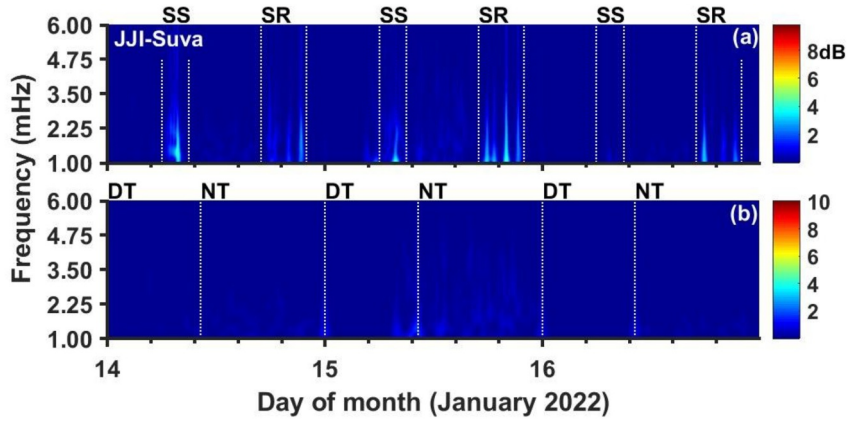

Figure 7. The wavelet spectra of JJI signal amplitude perturbations in the frequency range of 1–6 mHz presented in panels: (a) 24 hr (including terminator times marked as SS and SR) and (b) during daylight (DT, 00–06 UT) and night (NT, 09–17 UT) periods of the TRGCP, from 14 to 16 January 2022.

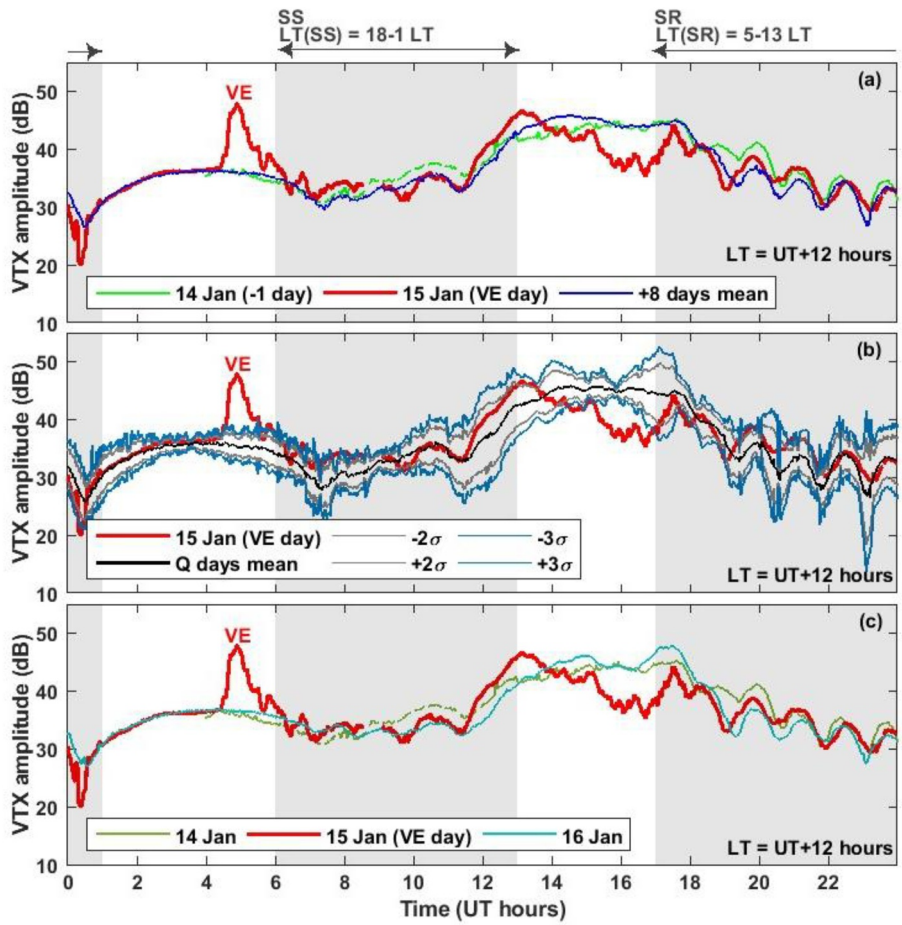

Figure 8. (a) VTX VLF signal amplitude variation in UT during 14–23 January 2022 which includes a day prior (−1 day, green line) and 8 days after (+8 days mean, blue line) the volcanic eruption on 15 January 2022 (red line), (b) the geomagnetically quiet (Q) days mean amplitude (black line), ±2σ (gray line) and ±3σ (blue line), and (c) a day prior (14 January) and a day after (16 January) the volcanic eruption day (15 January). Excursions in the amplitude outside ±2σ and ±3σ on 15 January 2022, are considered as VE-associated perturbations. The periods corresponding to sunset (SS) and sunrise (SR) transitions are indicated between the gray shaded region. LT = UT + 12 hr.

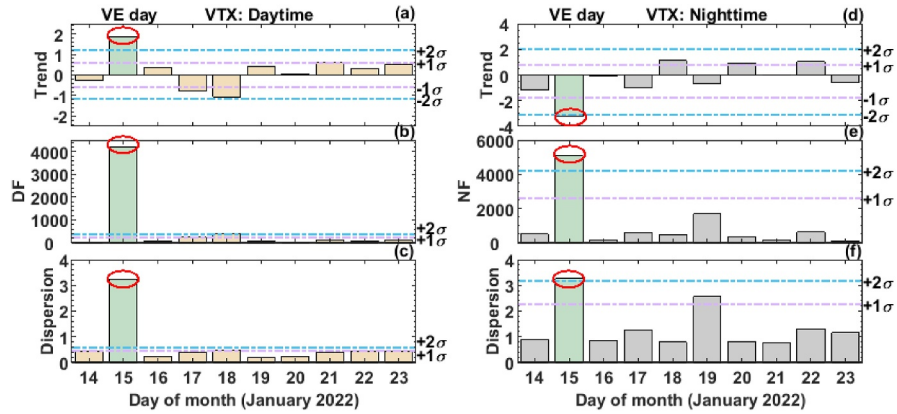

Figure 9. Graphical representation of the trend (a and d), fluctuation (b and e) and dispersion (c and f) in each panel for VTX VLF signal amplitude during the period from 14 to 23 January 2022. The panels (a–c) on the left side represent daytime while the panels (d–f) on the right side represent nighttime. The purple and blue horizontal dashed lines show the ±1σ and ±2σ criteria, respectively. The green bar represents the volcanic eruption day and the red circle on the bar indicates anomalous values on 15 January 2022 (values crossing the ±1σ and ±2σ lines).

marked as VE in Figures 8a–8c. A further check of the January 2021 VLF data (Figure S1b in Supporting Information S1) confirms that this strong signal enhancement was due to HTHH VE. VTX VLF signal phase variation during 14–16 January 2022 (Figure S3 in Supporting Information S1), showed a small increase (63°) in phase between the baseline and peak of the signal anomaly. Figure 9 shows a graphical representation of the trend (9a and 9d), fluctuation (9b and 9e) and dispersion (9c and 9f) in each panel for VTX VLF signal amplitude during the period from 14 to 23 January 2022. On VE day, the trend values during daytime and nighttime touched the ±2σ line (panel 9a and 9d). Likewise, fluctuation and dispersion (panel 9b, c, e and f) during the daytime and nighttime exceeded the +2σ line on VE day only.

Figures 10a and 10b show the H' (red) and β (blue) for the VTX signal path to Suva of the same duration and format as those presented in Figure 4a and b for the JJI signal. The pattern of variation in H' and β is almost the same for both signal paths. LWPC modeling results for path integrated perturbed H' and β values at peak of perturbed amplitude (shown in Figure 11) were estimated to be 73.8 km and 0.588 km^{-1}, respectively, showing a decrease in H' by 1.3 km and an increase in β by 0.286 km^{-1} from normal daytime values of $H' = 75.1$ km and $\beta = 0.302$ km^{-1} at 4:54 UT on 15 January. Figure 11 shows $Ne(h)$ versus ionospheric height in the height range of 70–90 km for the unperturbed and perturbed conditions denoted as a black dashed line and a red solid line, respectively. The electron density increased slightly at normal $h = 75.1$ km, but more strongly as h increased further. The $Ne(h)$ from 1.83×10^2 cm^{-3} at daytime normal $h = 75.1$ km increased to 3.94×10^2 cm^{-3}. The electron density under disturbed conditions at a height of 90 km increased from 1.94×10^2 cm^{-3} to 2.69×10^5 cm^{-3}, partly due to limitations as stated in the case of the JJI signal.

In Figures 12a and 12b, the Morlet wavelet analysis of VTX signal amplitude perturbations is presented for the same data format as in Figures 6a and 6b for the JJI transmitter. Figure 12a shows WLS around 0.5–0.25 mHz and comparatively weaker WLS in the range of 0.25–0.30 mHz on the VE day (15 January). Figure 12b shows wavelet analysis for pure daylight (5 hr per day) and night (4 hr per day) of VTX-Suva TRGCP. Due to this time duration limitation, we have filtered any WLS component below 0.14 mHz. Figure 12a shows WLS around 0.5–0.25 mHz and comparatively weaker WLS in the range of 0.25–0.30 mHz on the VE day (15 January). Weaker WLS in the range of 0.25–0.30 mHz on the VE day (15 January) extending into nighttime of 16 January were observed during the day (panel a). Figure 13a shows weak WLS in the range of 1–2 mHz with almost no WLS in Figure 13b during daytime and nighttime times of TRCP during 14–16 January 2022.

4. Discussion

The powerful VE of HTHH on 15 January 2022 created significant interest in the scientific community to study the connections between VE and its ionospheric effects (e.g., Astafyeva et al., 2022; Cahyadi et al., 2024; Li et al., 2023; Themens et al., 2022). Most studies have concentrated on the GNSSs given Total Electron Content

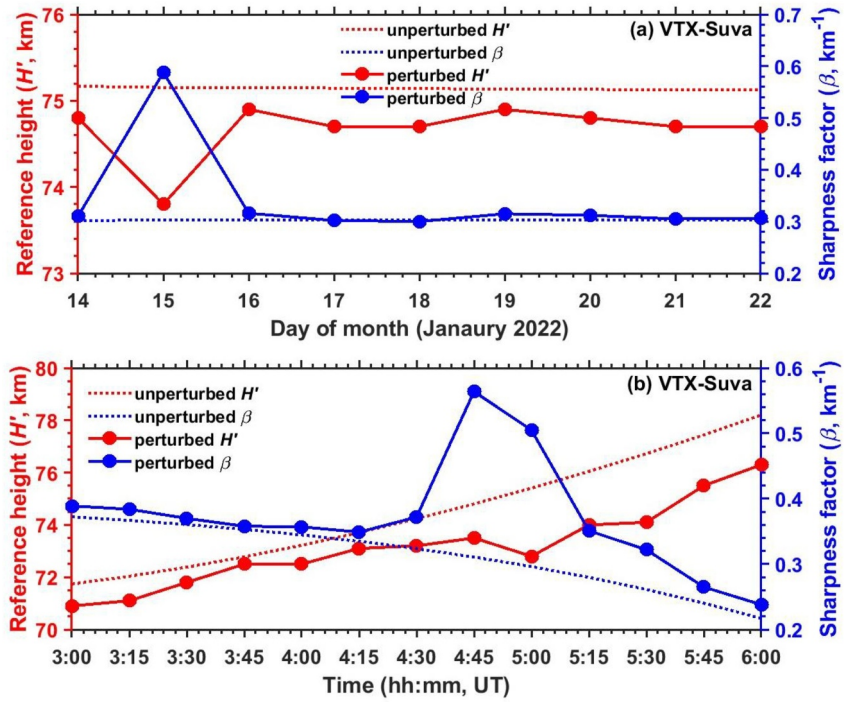

Figure 10. (a) Variation of the ionospheric Wait parameters: H' (red) and β (blue) associated with the daytime VTX to Suva signal every day at 4:54 UT from 8 to 22 January 2022 and (b) Temporal variation of the ionospheric Wait parameters associated with the daytime VTX to Suva signal from 3:00 to 6:00 UT (including signal anomaly) on 15 January 2022.

(TEC) based traveling ionospheric disturbances (TIDs) and various wave activities such as AGWs, AWs, Lamb waves (LWs), with observations made all over the globe (e.g., Harding et al., 2022; Themens et al., 2022). There could be two mechanisms for ionospheric changes: (a) an induced electric field and/or (b) the excitation of atmospheric and ocean waves (Tsunamis). The AGWs and AWs from VEs can travel into the ionosphere and cause TIDs. To date, TIDs associated with VEs have been reported using ionospheric observations using Ionosonde and GNSS receiver networks (e.g., Huang et al., 2019). While GNSS-based integrated TEC measurements have provided much wider coverage of strong eruption-related ionospheric perturbations, they lag in providing purely lower ionospheric (D-region) changes. VLF radio waves provide a unique opportunity as diagnostic tools for lower ionospheric changes, the wave-like nature of lower ionospheric TIDs, and the wave activity associated with VEs. The first attempt at sub-ionospheric VLF measurements using the Pacific network of VLF receivers was made by Rozhnoi et al. (2014) for 26–30 January 2011 strong VEs, which occurred at Shinmoe-dake of the Kirishima volcanic group (31.912°N, 130.883°E) located in the Kyushu Island of Japan. During Shinmoe-dake's subsequent pre-eruptive and eruptive activity, they observed only nighttime VLF signal anomalies of 5–6 dB. They attributed VLF perturbations to the internal AGWs of periods 6–30 min. A few research/reports have been done on the VLF perturbations associated with HTHH VE. Solovieva et al. (2022) studied ionospheric perturbations using VLF, LF and GNSS Radio Sounding. For VLF and LF sounding, they used NWC (VLF, 19.8 kHz) and JJY (LF, 40 kHz) transmitter signals received at the Petropavlovsk-Kamchatsky (PTK) station in Russia. They reported nighttime VLF perturbations of about 1–2 dB and attributed these VLF perturbations to AGWs, followed by LWs and Tsunami waves. Solovieva and Shalimov (2022) extended the above study using JJY and NPM (21.4 kHz) signals and reported VLF perturbations due to LWs and Tsunami waves. Ohya et al. (2024), using VLF/LF (3–30/30–300 kHz) transmitter signals, atmospheric electric field data, ground-based magnetic field data, and ground-level atmospheric pressure data to

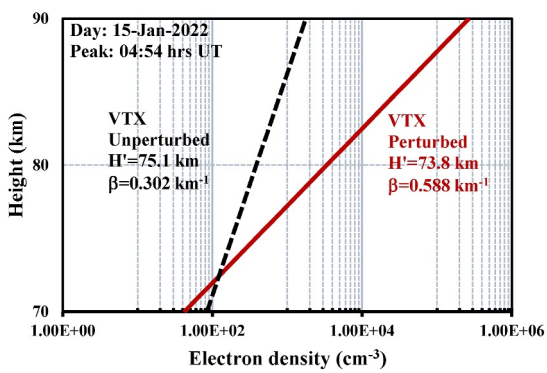

Figure 11. The perturbed electron density of the volcanic eruption on 15 January 2022 with a peak at 04:54 UT for the VTX (red solid line) compared with the normal unperturbed electron density for VTX (black dashed line) to the Suva path in the altitude range of 70–90 km.

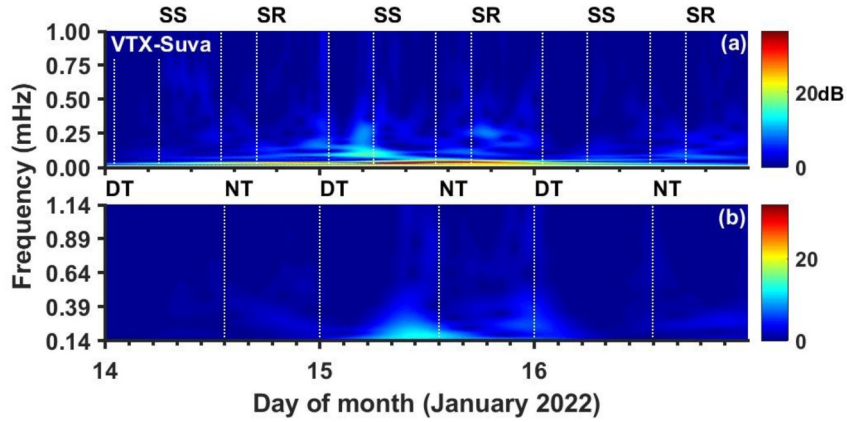

Figure 12. The wavelet spectra of VTX signal amplitude perturbations in the frequency range of 00–1.0 mHz presented in panels: (a) 24 hr (including terminator times marked as SS and SR) and (b) during daylight (DT, 01–06 UT) and night (NT, 13–17 UT) periods of the TRGCP, during 14–16 January 2022.

determine the D-region electron density changes associated with HTHH VE. They used the JJI VLF transmitter and the JJY low frequency (LF, 60 kHz) transmitter at BPC (34.63°N, 115.83°E, 68.5 kHz), China, signals recorded at Tainan (23.06°N, 120.15°E), Taiwan, having a long distance ∼8,000–10,000 km between the HTHH location and VLF/LF propagation paths. They accounted for variations in the VLF and LF signals to changes in the D-region ionosphere associated with AGWs, LWs and Pekeris waves, which contributed significantly due to acoustic resonance.

However, our observations of HTHH VE show large daytime VLF perturbations (11.1 dB on JJI and 12.6 dB on VTX) during the daytime of the TRGCPs of both the signals (JJI and VTX) to Suva, and perturbations extended well into the nighttime of 15 January 2022 at a reduced level. This shows that AGWs originating from the HTHH VE and migrating by LWs had an impact over a long period of time (∼ several hours) consistent with F-region observations (e.g., Liu et al., 2023; Miyoshi & Shinagawa, 2023; Vadas et al., 2023; Wu et al., 2023). Since the daytime lower ionosphere is stable, the larger anomalies demonstrate a strong effect of HTHH VE on the lower ionosphere. Additionally, LWPC modeling of VLF perturbations gives a large decrease in H' by 3.2 km and an increase in β by 0.319 km^{-1} due to a significant increase in the D-region electron density. Strong long-duration VLF perturbations are reported here due to HTHH VE associated significant changes in the D-region electron density. The JJI signal gives a large decrease in the H' due to the occurrence of the event during the daytime due to diffusive reflection from the enhanced electron density of the D-region. The unusually strong amplitude

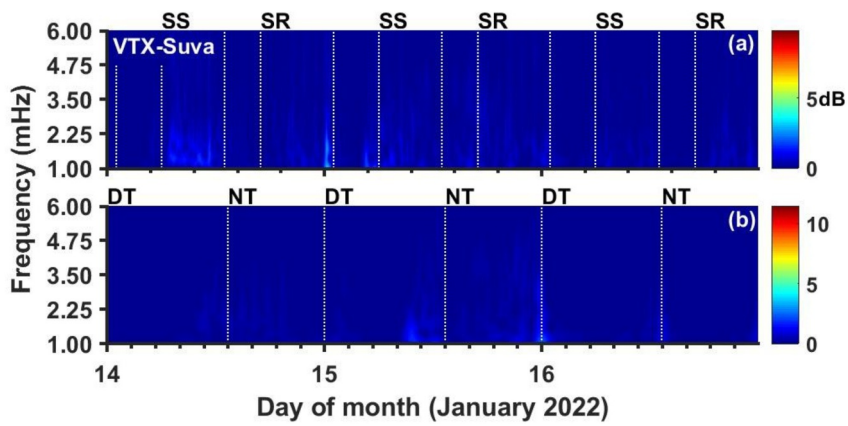

Figure 13. Wavelet spectra of VTX signal amplitude perturbations in the frequency range of 1–6 mHz presented in panels: (a) 24 hr (including terminator times marked as SS and SR) and (b) during daylight (DT, 01–06 UT) and night (NT, 13–17 UT) periods of the TRGCP, during 14–16 January 2022.

anomalies (11.1, 12.6 dB) of the JJI and VTX signals are consistent with the high volcanic explosivity index of six for the modern era's largest HTHH VE.

The three statistical parameters of the VLF propagation, trend (T), fluctuation (F) and dispersion (D) are widely used in earthquake analysis where the anomaly is considered by the simultaneous decrease in the T and rise in the F and D (Hayakawa et al., 2010; S. Kumar et al., 2013, 2022). We applied the same method to the HTHH VE for the daytime and nighttime VLF signals. From our analysis of the JJI signal, an increase in daytime fluctuation (DF) and D during both daytime and nighttime on the VE day reached above the $+2\sigma$ mark. For the VTX signal, the nighttime T showed a decrease, while daytime T, daytime and nighttime F and daytime and nighttime D showed an increase during the VE day. The T of the VTX signal showed a decrease in the average of nighttime dA (t) values on the VE days due to the reduction in the ionospheric VLF reference height. The nighttime fluctuation level is the integral of $[dA(t)]^2$ values over the individual nighttime hours. Dispersion is the standard deviation of dA(t) values for each day and was found to exceed $+2\sigma$ mark on VE day because of its large variability from a standard average value. The anomalies in the T, F and D observed in the VLF signal amplitude are due to acoustic and gravity wave channels and the direct effect of strong lightnings associated with HTHH VE. These are produced near the VE zone and move upward to the ionosphere and later alter the properties of the ionosphere.

The long duration existence of VLF perturbations well into the nighttime can also be accounted for by atmospheric AGWs due to exceptionally intense volcanic lightning detected by the Global Lightning Detection Network (GLD360) in the rapidly expanding volcanic plume of HTHH VE (Ichihara et al., 2023; Mezentsev et al., 2023; Yuen et al., 2022). Briggs et al. (2022) reported significantly enhanced lightning rates between 04:10 UT and 06:20 UT with a peak around 04:57 UT which again increased moderately between 08:00 UT and 09:15 UT detected by the World Wide Lightning Location Network (WWLLN) within a 400 km radius of the HTHH VE. Using Schumann resonance and WWLLN data, Mezentsev et al. (2023) reported roughly 400,000 lightning strikes from 05:19–10:00 UT (18:19–23:00 LT, Tonga). GLD360 detected a sharp increase in lightning activity from 04:35 UT, which peaked at about 05:10 UT on 15 January (Yuen et al., 2022), with another remarkable peak activity between 05:36 and 05:50 UT. Jarvis et al. (2023), based on GLD360 reported unprecedented intensity of volcanic lightning during the HTHH eruption with over 3×10^5 strikes over a 2-hr period. They also reported that about 20 min after the eruption onset, a radial structure appeared in the lightning spatial distribution, with strikes clustered both directly above HTHH and in an annulus of radius ∼50 km. The strong lightning strokes can directly cause extra ionization of the D-region from which short duration (∼100 s) VLF perturbations associated with narrow-angle scattering from extra ionization generated by lightning discharges occurring at distances of about ±50 km off the transmitter receiver great circle path (TRGCP) and by wide-angle scattering by lightning discharges occurring at distances of less than 500 km off the TRCGP and around the receiver are observed (S. Kumar et al., 2008; Rodger, 2003). This is not the case here as the duration of HTHH VE associated anomalies on JJI and VTX signals is of much longer duration (∼2 hr, 04:28–06:24 UT) than that produced by direct D-region effects of individual lightning strokes associated with short duration (∼100 s) extra ionization. However, strong lightning discharges can produce strong ionization with longer recoveries of 5–20 min (Cotts & Inan, 2007; Haldoupis et al., 2013; S. Kumar & Kumar, 2013; Salut et al., 2012) and sustained/successive strong dynamic lightnings can also produce longer duration ionization due to strong quasi electric (QE) fields and electromagnetic pulses (EMPs) emitted by strong discharges hence the VLF anomalies. The VLF perturbations strongly depend on both the magnitude and polarity (positive/negative cloud-to-ground) of the causative lightning peak current and the energy of lightning strokes (Chand et al., 2023; Salut et al., 2013). Based on the theoretical models, Cho and Rycroft (1998) showed that strong lightning EMPs can induce changes in ionization in the lower ionosphere, which can last for many minutes. Barrington-Leigh and Inan (1999) reported that even a single EMP can affect a large area ($\sim 3 \times 10^5$ km^2) at the D-region altitude, causing significant changes in the electron density. Rodger et al. (2001) showed that successive intense lightning EMPs can produce significantly large-scale ionization changes in the nighttime lower ionosphere by 100% or even greater with the largest increases at 90 km altitude. The lightning associated perturbations are most common at nighttime but can also occur during daylight (S. Kumar & Kumar, 2013; S. Kumar et al., 2008). Thus, the extra ionization produced due to successive strong dynamic lightnings associated with the HTHH volcanic activity has contributed to unusually strong VLF signal anomalies (amplitude increase) through the constructive interference of the direct VLF signal and scattered signal scattered at the receiver due to narrow-angle scattering (Inan et al., 1995) or wide-angle including backscattering (S. Kumar & Kumar, 2013; Rodger, 2003). Based on satellite-based Geostationary Lightning Mapper (GLM) onboard GOES-17, GLD360, Earth Networks Total Lightning Network (ENTLN), and WWLLN data sets, Van

Eaton et al. (2023) reported an astonishing rate of volcanic lightning (>2,600 flashes min $^{-1}$) with earliest lightning on 15 January at ∼04:09 UT, flashes from 04:14–04:25 UT and most significant number of optically detected flashes occurred from 12:17–15:21 UT. They also reported AGWs associated with lightning, which by 04:47 UT was >10 km high from peak to trough and moved outward at speeds >80 m s^{-1}. The strong lightnings associated with AGWs would have contributed to the VLF anomalies and further fluctuations in VLF signals observed until 16–17 UT on 15 January (Figures 2 and 8). Thunderstorms are the natural powerful sources of atmospheric waves, mainly the infrasonic waves at periods 20–50 s activity and they also produce AGWs associated with deep convection inside thunderstorm structures (Blanc et al., 2014; Sentman et al., 2003) and can propagate vertically into the stratosphere, mesosphere, and lower thermosphere (Ionosphere), affect the general atmospheric circulation (Baldwin et al., 2003; Pasko et al., 1997) and generate TIDs.

Apart from the volcanic eruptions, the lower ionosphere can be greatly influenced from below by tropical cyclones (TCs) (S. Kumar et al., 2017) and from above by solar flares and geomagnetic storms (e.g., S. Kumar et al., 2015, 2023; Thomson et al., 2004, 2005). There were no TCs active around both the HTHH eruption and the Suva station and around the paths of JJI and VTX signals to Suva. There were no solar flares of class C or above around the time of the eruption occurrence on 15 January. However, an M1.8 class solar flare occurred on 14 January, starting at 01:47 UT and ending at 02:14 UT, well before the HTHH VE occurrence. These flares produced an enhancement in the signal amplitude for their duration (not shown here) on 14 January. There also occurred a geomagnetic storm of moderate strength (minimum $Dst = -91$ nT) on 14 January. The *Dst* index variation obtained from World Data Center (WDC), Geomagnetic Data Services, Kyoto, Japan, http://wdc.kugi.kyoto-u.ac.jp/wdc/Sec3.html showed that the main phase of the storm occurred between 16 and 23 UT on 14 January and the recovery phase during 15–16 January. There were no VLF perturbations observed during this storm's main and recovery phases before the occurrence of the HTHH VE at 04:08 UT during the recovery phase of this storm. A geomagnetic storm of such strength can cause some changes in the upper ionosphere, but it is highly unlikely to cause any changes in the D-region, particularly during the recovery phase of the storm (S. Kumar et al., 2023). We further examined ±3 months of the *Dst* index data from the VE month (January 2022) and found a storm of similar strength during 3–5 November 2021 with a minimum *Dst* index of −105 nT. Although this storm was a bit stronger than the 14 January 2022 storm, but it did not produce any noticeable VLF perturbations (signal analysis not presented here) in both JJI and VTX signals during both the main and recovery phases of this storm. In contrast to the unusually large sharp increase in VLF signal strength associated with HTHH VE, storm effects are weaker and build gradually with a decrease in the signal strength for a longer period, as found by S. Kumar et al. (2015) for 14–16 December 2006 with a minimum *Dst* index −146 nT. S. Kumar et al. (2023) conducted a comprehensive analysis of the effects of 12 intense storms, from 2011 to 2016 and 2018, on NWC, NPM, and NLK VLF signals monitored at a low-latitude station in Suva, Fiji. They found that 7 out of 12 geomagnetic storms revealed VLF anomalies during the storm main phase and storm recovery phase days, which were mainly characterized by smooth decreases in VLF amplitudes. Earlier studies also indicated minimal impacts of 14 January 2022 geomagnetic storm on TEC measurements (e.g., Li et al., 2023). Thus, the D-region perturbations and VLF anomalies reported here on JJI, and VTX VLF signals are accounted for the HTHH VE of 15 January 2022. A delay of 20–27 min between the start of VLF perturbations (04:28 UT on JJI and 04:35 UT on VTX) and about 50 min delay from the peak of anomaly (04:58 UT on JJI and VTX) and VE occurrence at 04:08 UT can be accounted for the propagation delays of HTHH VE-associated AGWs to the D-region altitudes over the HTHH VE location and of TRGCPs of these signals from the commencement of AGWs due to HTHH VE and causing the maximum perturbations. The unusually strong positive signal amplitude anomalies of >10 dB presented here are explained by constructive interference at the receiver location between the direct VLF signal and the scattered signal from D-region ionization enhancement due to HTHH VE. Moreover, Figure 14 shows the atmospheric pressure variation from 14 to 16 January 2025 recorded at a station MSVF located in Monasavu, Fiji. On 15 January, a clear strong pressure fluctuation was recorded after the HTHH VE that started at 04:43 UT and increased to a maximum of ∼845.7 Pa at 05:09 UT and decreased to ∼−644.7 Pa at 05:18 UT, lasting between 04:43–07:56 UT, indicating that the atmospheric waves generated by the HTHH eruption arrived in Fiji during the signal anomaly between 04:28 and 06:24 UT. Matoza et al. (2022), using ground-based and spaceborne instrumentation networks, have reported atmospheric and global seismo-acoustic waves associated with HTHH VE. They reported that this eruption produced remarkable globally detected infrasound (0.01–20 Hz), long-range (∼10,000 km) audible sound, and ionospheric perturbations with the most prominent observations of surface-guided LWs (≲0.01 Hz), which propagated for four (plus three antipodal) passages around the Earth over 6 days.

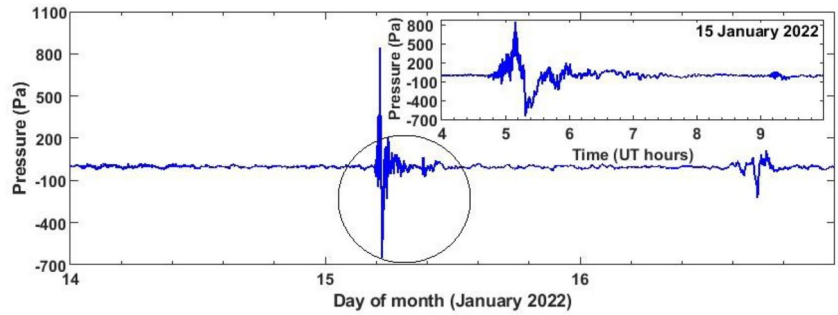

Figure 14. Atmospheric pressure variation from 14 to 16 January 2025 at the station in Monasavu, Fiji, during 14–16 January 2022. The black circle represents the pressure fluctuations due to the HTHH volcanic eruption and its zoom view from 04:00 UT to 09:00 UT on 15 January is also shown in this plot.

In the lower atmosphere, AWs have frequencies greater than the acoustic cutoff frequency (3.3 mHz) and AGWs have frequencies lower than the Brunt-Väisälä frequency (~2.9 mHz) (Astafyeva, 2019). AGWs can significantly couple energy and momentum from the lower to the upper atmosphere/ionosphere (Fritts & Alexander, 2003). The wave frequencies estimated from wavelet spectrograms presented in Figures 6 and 12 are in the range of 0.02–0.45 mHz, showing that VLF/D-region perturbations were mainly associated with low-frequency or long period (~37 min–5.55 hr) internal/atmospheric AGWs excited by significant convection and heating associated with this VE (Holton et al., 2002). This seems to have included low-frequency LWs as the frequency (≤0.01 Hz) range of the LWs is between ~0.2 and 10 mHz (Nishida et al., 2014). LWs are acoustic waves that propagate non-depressively in the horizontal direction near the Earth's surface, with a phase velocity of ~310 ms^{-1}. LWs while propagating horizontally in the lower atmosphere (troposphere) can leak their energy into higher altitudes (including the ionosphere) (Ghent & Crowell, 2022; Nishida et al., 2014). The HTHH VE triggered a wide spectrum of waves, including AGWs propagating at 238 ± 3 to 269 ± 3 m s^{-1} in the stratosphere and LWs propagating at phase speeds of 318.2 ± 6 m s^{-1} at surface level and between 308 ± 5 and 319 ± 4 m s^{-1} in the stratosphere (Wright et al., 2022). Considering these velocities, the AGWs will take about 43–49 min to arrive at the receiver site, and LWs will take about 36.5–38 min, which from the HTHH VE start time of 04:00 UT, will be during the VLF anomalies observed during 04:28 to 06:24 UT. Ravanelli et al. (2023) have attributed ionospheric TEC variation over the New Caledonia-New Zealand region to LWs associated with HTHH VE. Based on VLF (JJI) and LF (JJY) transmitter signal variations due to HTHH VE observed at Tainan, Taiwan, Ohya et al. (2024) have shown the D-region changes associated with AGWs, LWs and Pekeris waves. Also, our wavelet analysis showed no signatures of AWs, which is consistent with the results presented by Muafiry et al. (2023) based on TEC observations over the New Zealand region. Strong long-duration VLF perturbations (Figures 2 and 8) and, hence, the D-region ionosphere were also due to low-frequency internal/atmospheric AGWs associated with HTHH VE, which changed D-region electron density via dynamical (fluctuations in the D-region by lifting and sinking it to lower/higher recombination rates) and altering photochemical processes (Astafyeva, 2019; George & Hooke, 1970). George and Hooke (1970) have reported that neutral waves can significantly alter photochemical balance at lower altitudes (below 250 km), which includes the lower ionosphere (D-region). Astafyeva (2019) using satellite observations in South America had reported concentric AGWs generated by a volcanic eruption in South America. Thus, the integrated effect of long duration strong ionization produced by the sustained highest concentration of lightnings ever recorded (Bor et al., 2023; Van Eaton et al., 2023) and AGWs and LWs associated with HTHH VE are reported here, causing unusually strong VLF amplitude anomalies and D-region electron density changes presented in this study. This study presents the first comprehensive examination of the D-region changes due to HTHH VE, considering any severe space (geomagnetic storms and solar flares) and extreme terrestrial (tropical cyclones, lightning discharges) weather events and wave activity that may have impacted the lower ionosphere in the South Pacific Region.

5. Summary and Conclusions

We have presented a study on strong daylight VLF signal anomalies of 11.1 and 12.6 dB on the JJI and VTX signals, respectively, and associated D-region changes, observed at Suva, Fiji, following the extraordinary VE of HTHH on 15 January 2022. Modeling of JJI VLF anomalies using the LWPC code 2.1 gives a large decrease in

D-region H' of up to 3.2 km and an increase in β of 0.319 km^{1}, giving an electron density increase from 1.83×10^{2} cm^{-3} to 1.34×10^{3} cm^{-3} values at the normal daytime H' of 75.1 km. The statistical analysis of trend, fluctuation and dispersion of VLF amplitude anomalies due to lower ionospheric changes were associated with the HTHH VE. These are produced near the VE and moved upward to the ionosphere, altering D-region properties. The eruption and its associated lightnings produced extra ionization in the large area due to successive strong lightnings and associated AGWs lifting and sinking the density of the mesosphere and lower thermosphere, resulting in changes in the photochemical processes, which are mediated mainly by AGWs of frequency 0.10–0.30 mHz obtained using Morlet wavelet analysis of VLF perturbations associated with HTHH VE. Based on this frequency range of WLS obtained from 24-hr continuous data analysis (Figures 6a and 12a) and published results (Wright et al., 2022), a contribution of LWs is also suggested, as their energy can leak into higher altitudes (including lower ionosphere) and cause D-region changes. Based on several studies reported on the ionosphere using TEC in association with the HTHH VE, the results of this study demonstrate coupling between the upper ionosphere, D-region ionosphere, and neutral atmosphere due to AGWs and LWs generated by the HTHH VE. Both VLF signals fluctuated throughout the night of 15 January following the occurrence of HTHH VE, indicating that wave-like disturbance took a long time to subside the D-region ionosphere to return to its normal state, which may also be accounted for the AGWs due to substantially enhanced lightning strikes from 05:19–10:00 (18:19–23:00 LT, Tonga) in the volcanic plume of HTHH VE.

Conflict of Interest

The authors declare no conflicts of interest relevant to this study.

Data Availability Statement

The narrowband VLF data used in the present study are available at the Zenodo Research Data Repository and can be obtained from S. Kumar (2024). The *Dst* and *Kp* indices data were obtained from the World Data Center, Kyoto University, Kyoto, Japan (online at http://wdc.kugi.kyoto-u.ac.jp/wdc/Sec3.html) and atmospheric pressure from EarthScope Consortium Wed Services (https://service.iris.edu/).

Acknowledgments
The authors are also thankful for the financial support from The University of the South Pacific's main Research Office under the Strategic Research Theme (Grant F7304-RI001-ACC-001) under which this work was carried out. This study was also supported by the Science and Technology Research Partnership for Sustainable Development (SATREPS), funded by Japan International Cooperation Agency (JICA)/Japan Science and Technology Agency (JST) (Grant 23727132). The *Dst* and *Kp* index values were obtained from the World Data Centre, Kyoto University, Kyoto, Japan (online at https://wdc.kugi.kyoto-u.ac.jp/wdc/Sec3.html). The atmospheric pressure data were downloaded through the EarthScope Consortium Web Services (https://service.iris.edu/).

References

Astafyeva, E. (2019). Ionospheric detection of natural hazards. *Reviews of Geophysics*, *57*(4), 1265–1288. https://doi.org/10.1029/2019RG000668

Astafyeva, E., Maletckii, B., Mikesell, T. D., Munaibari, E., Ravanelli, M., Coisson, P., et al. (2022). The 15 January 2022 Hunga Tonga eruption history as inferred from ionospheric observations. *Geophysical Research Letters*, *49*(10), e2022GL098827. https://doi.org/10.1029/2022GL098827

Baldwin, M. P., Thompson, D. W. J., Shuckburgh, E. F., Norton, W. A., & Gillet, N. P. (2003). Weather from the stratosphere? *Science*, *301*(5631), 317–319. https://doi.org/10.1126/science.1085688

Barrington-Leigh, C., & Inan, U. S. (1999). Elves triggered by positive and negative lightning discharges. *Geophysical Research Letters*, *26*(6), 683–686. https://doi.org/10.1029/1999gl900059

Blanc, E., Farges, T., Pichon, A. L., & Heinrich, P. (2014). Ten year observations of gravity waves from thunderstorms in western Africa. *Journal of Geophysical Research: Atmospheres*, *119*, 6409–6418. https://doi.org/10.1002/2013JD020499

Bor, J., Bozoki, T., Satori, G., Williams, E., Behnke, S. A., Rycroft, M. J., et al. (2023). Responses of the AC/DC global electric circuit to volcanic electrical activity in the Hunga Tonga-Hunga Ha'apai eruption on 15 January 2022. *Journal of Geophysical Research: Atmospheres*, *128*(8), e2022JD038238. https://doi.org/10.1029/2022JD038238

Briggs, M. S., Lesage, S., Schultz, C., Mailyan, B., & Holzworth, R. H. (2022). A terrestrial gamma-ray flash from the 2022 Hunga Tonga–Hunga Ha'apai volcanic eruption. *Geophysical Research Letters*, *49*(14), e2022GL099660. https://doi.org/10.1029/2022GL099660

Cahyadi, M. N., Muslim, B., Muafiry, I. N., Gusman, A. R., Handoko, E. Y., Anjasmara, I. M., et al. (2024). 3D traveling ionospheric disturbances during the 2022 Hunga Tonga–Hunga Ha'apai eruption using GNSS TEC. *Journal of Geophysical Research: Space Physics*, *129*(3), e2023JA031806. https://doi.org/10.1029/2023JA031806

Chand, A. E., Kumar, A., & Kumar, S. (2023). VLF and ionospheric D-region perturbations associated with WWLLN-detected lightning in the South Pacific Region. *Journal of Geophysical Research: Space Physics*, *128*(4), e2022JA030964. https://doi.org/10.1029/2022JA030964

Cho, M., & Rycroft, M. J. (1998). Computer simulation of the electric field structure and optical emission from cloud-top to the ionosphere. *Journal of Atmospheric and Solar-Terrestrial Physics*, *60*(7–9), 871–888. https://doi.org/10.1016/s1364-6826(98)00017-0

Cotts, B. R. T., & Inan, U. S. (2007). VLF observation of long ionospheric recovery events. *Geophysical Research Letters*, *34*(14), L14809. https://doi.org/10.1029/2007GL030094

Cummer, S. A., Inan, U. S., & Bell, T. F. (1998). Ionospheric D region remote sensing using VLF radio atmospherics. *Radio Science*, *33*(6), 1781–1792. https://doi.org/10.1029/98rs02381

Duncombe, J. (2022). The surprising reach of Tonga's giant atmospheric waves. *Eos*, *103*. https://doi.org/10.1029/2022eo220050

Ferguson, J. (1998). *Computer programs for assessment of long-wavelength radio communications, Version 2.0: User's guide and source files*. Rep. Space and Naval Warfare Systems Center.

Fritts, D. C., & Alexander, M. J. (2003). Gravity wave dynamics and effects in the middle atmosphere. *Reviews of Geophysics*, *41*(1), 1003. https://doi.org/10.1029/2001RG000106

George, T. M., & Hooke, W. H. (1970). Wave-induced fluctuations in ionospheric electron content: A model indicating some observational biases. *Journal of Geophysical Research*, *75*(31), 6295–6308. https://doi.org/10.1029/JA075i031p06295

Ghent, J. N., & Crowell, B. W. (2022). Spectral characteristics of ionospheric disturbances over the southwestern Pacific from the 15 January 2022 Tonga eruption and tsunami. *Geophysical Research Letters*, *49*(20), e2022GL100145. https://doi.org/10.1029/2022GL100145

Haldoupis, C., Cohen, M., Arnone, E., Cotts, B., & Dietrich, S. (2013). The VLF fingerprint of elves: Step-like and long-recovery early VLF perturbations caused by powerful ±CG lightning EM pulses. *Journal of Geophysical Research: Space Physics*, *118*(8), 5392–5402. https://doi.org/10.1002/jgra.50489

Harding, B. J., Wu, Y. J. J., Alken, P., Yamazaki, Y., Triplett, C. C., Immel, T. J., et al. (2022). Impacts of the January 2022 Tonga volcanic eruption on the ionospheric dynamo: ICON-MIGHTI and Swarm observations of extreme neutral winds and currents. *Geophysical Research Letters*, *49*(9), e2022GL098577. https://doi.org/10.1029/2022GL098577

Hayakawa, M., Kasahara, Y., Nakamura, T., Muto, F., Horie, T., Maekawa, S., et al. (2010). A statistical study on the correlation between lower ionospheric perturbations as seen by subionospheric VLF/LF propagation and earthquakes. *Journal of Geophysical Research*, *115*(A9). https://doi.org/10.1029/2009JA015143

Hines, C. O. (1960). Internal atmospheric gravity waves at ionospheric heights. *Canadian Journal of Physics*, *38*(11), 1441–1481. https://doi.org/10.1139/p60-150

Holton, J. R., Beres, J. H., & Zhou, X. (2002). On the vertical scale of gravity waves excited by localized thermal forcing. *Journal of the Atmospheric Sciences*, *59*(12), 20192–22023. https://doi.org/10.1175/1520-0469(2002)059<2019:OTVSOG>2.0.CO;2

Horiuchi, T., Ichihara, M., Nishida, K., & Kaneko, T. (2024). A seismic precursor 15 min before the giant eruption of Hunga Tonga-Hunga Ha'apai volcano on 15 January 2022. *Geophysical Research Letters*, *51*(21), e2024GL111144. https://doi.org/10.1029/2024GL111144

Huang, C. Y., Helmboldt, J. F., Park, J., Pedersen, T. R., & Willeman, R. J. (2019). Ionospheric detection of explosive events. *Reviews of Geophysics*, *57*(1), 78–105. https://doi.org/10.1029/2017rg000594

Ichihara, M., Mininni, P. D., Ravichandran, S., Cimarelli, C., & Chris Vagasky, C. (2023). Multiphase turbulent flow explains lightning rings in volcanic plumes, communications. *Earth and Environment*, *4*(1), 417. https://doi.org/10.1038/s43247-023-01074-z

Igarashi, K., Kainuma, S., Nishmuta, I., Okamoto, S., Kuroiwa, H., Tanaka, T., & Ogawa, T. (1994). Ionospheric and atmospheric disturbances around Japan caused by the eruption of Mount Pinatubo on June 15, 1991. *Journal of Atmospheric and Terrestrial Physics*, *56*, 1227.

Inan, U. S., Bell, T. F., Pasko, V. P., Sentman, D. D., Wescott, E. M., & Lyons, W. A. (1995). VLF signatures of ionospheric disturbance associated with sprites. *Journal of Geophysical Research*, *22*(24), 3461–3464. https://doi.org/10.1029/95gl03507

Jarvis, P. A., Caldwell, T. G., Noble, C., Ogawa, Y., & Vagasky, C. (2023). Volcanic lightning reveals umbrella cloud dynamics of the 15 January 2022 Hunga volcano eruption, Tonga. *Bulletin of Volcanology*, *86*(6), 54. https://doi.org/10.1007/s00445-024-01739-3

Kulichkov, S., Chunchuzov, I., Popov, O., Gorchakov, G., Mishenin, A., Perepelkin, V., et al. (2022). Acoustic-gravity lamb waves from the eruption of the Hunga-Tonga-Hunga-Hapai volcano, its energy release and impact on aerosol concentrations and tsunami. *Pure and Applied Geophysics*, *179*(5), 1–16. https://doi.org/10.1007/s00024-022-03046-4

Kumar, A., & Kumar, S. (2020). Ionospheric D region parameters obtained using VLF measurements in the South Pacific region. *Journal of Geophysical Research: Space Physics*, *125*(1), e2019JA027536. https://doi.org/10.1029/2019JA027536

Kumar, A., Kumar, S., Hayakawa, M., & Menk, F. (2013). Subionospheric VLF perturbations observed at low latitude associated with earthquake from Indonesia region. *Journal of Atmospheric and Solar-Terrestrial Physics*, *102*, 71–80. https://doi.org/10.1016/j.jastp.2013.04.011

Kumar, S. (2024). VLF anomalies observed in Fiji associated with Tonga Volcanic Eruption of 15 January 2022 [Dataset]. *Zenodo*. https://zenodo.org/records/11336159

Kumar, S., Dixit, S. K., & Gwal, A. K. (1994). Propagation of tweek atmospherics in the Earth-ionosphere waveguide. *Nuovo Cimento A*, *17*(3), 275–281. https://doi.org/10.1007/bf02509168

Kumar, S., & Kumar, A. (2013). Lightning-associated VLF perturbations observed at low latitude: Occurrence and scattering characteristics. *Earth Planets and Space*, *65*(1), 25–37. https://doi.org/10.5047/eps.2012.05.019

Kumar, S., Kumar, A., Menk, F., Maurya, A. K., Singh, R., & Veenadhari, B. (2015). Response of the low-latitude D region ionosphere to extreme space weather event of 14–16 December 2006. *Journal of Geophysical Research: Space Physics*, *120*(1), 788–799. https://doi.org/10.1002/2014JA020751

Kumar, S., Kumar, A., & Rodger, C. J. (2008). Subionospheric early VLF perturbations observed at Suva: VLF detection of red sprites in the day? *Journal of Geophysical Research*, *113*(A3), A03311. https://doi.org/10.1029/2007JA012734

Kumar, S., Kumar, S., & Kumar, A. (2022). Earthquakes associated subionospheric VLF anomalies recorded at two low latitude stations in the South Pacific region. *Journal of Atmospheric and Solar-Terrestrial Physics*, *229*, 105834. https://doi.org/10.1016/j.jastp.2022.105834

Kumar, S., Kumar, S., & Singh, R. (2023). Geomagnetic storm associated D-region anomalies estimated from VLF observations at a low-latitude station, Suva, Fiji. *Journal of Geophysical Research: Space Physics*, *128*(10), e2022JA031253. https://doi.org/10.1029/2022JA031253

Kumar, S., NaitAmor, S., Chanrion, O., & Neubert, T. (2017). Perturbations to the lower ionosphere by tropical cyclone Evan in the South Pacific Region. *Journal of Geophysical Research: Space Physics*, *122*(8), 8720–8732. https://doi.org/10.1002/2017JA024023

Li, R., Lei, J., Kusche, J., Dang, T., Huang, F., Luan, X., et al. (2023). Large-scale disturbances in the upper thermosphere induced by the 2022 Tonga volcanic eruption. *Geophysical Research Letters*, *50*(3), e2022GL102265. https://doi.org/10.1029/2022GL102265

Liu, L., Morton, Y., Cheng, P.-H., Amores, A., Wright, C. J., & Hoffmann, L. (2023). Concentric traveling ionospheric disturbances (CTIDs) triggered by the 2022 Tonga volcanic eruption. *Journal of Geophysical Research: Space Physics*, *128*(2), e2022J56. https://doi.org/10.1029/2022JA030656

Mallat, S. (1999). *A wavelet tour of signal processing*. Elsevier.

Matoza, R. S., Fee, D., Assink, J. D., Iezzi, A. M., Green, D. N., Kim, K., et al. (2022). Atmospheric waves and global seismoacoustic observations of the January 2022 Hunga eruption, Tonga. *Science*, *377*(6601), 95–100. https://doi.org/10.1126/science.abo7063

McRae, W. M., & Thomson, N. R. (2000). VLF phase and amplitude: Daytime ionospheric parameters. *Journal of Atmospheric and Solar-Terrestrial Physics*, *62*(7), 609–618. https://doi.org/10.1016/S1364-6826(00)00027-4

Mezentsev, A., Nickolaenko, A. P., Shvets, A. V., Galuk, Y. P., Schekotov, A. Y., Hayakawa, M., et al. (2023). Observational and model impact of Tonga volcano eruption on Schumann resonance. *Journal of Geophysical Research: Atmospheres*, *128*(7), e2022JD037841. https://doi.org/10.1029/2022JD037841

Miyoshi, Y., & Shinagawa, H. (2023). Upward propagation of gravity waves and ionospheric perturbations triggered by the 2022 Hunga-Tonga volcanic eruption. *Earth Planets and Space*, *75*(1), 68. https://doi.org/10.1186/s40623-023-01827-2

Muafiry, I. N., Wijaya, D. D., Meilano, I., & Heki, K. (2023). Diverse ionospheric disturbances by the 2022 Hunga Tonga-Hunga Ha'apai eruption observed by a dense GNSS array in New Zealand. *Journal of Geophysical Research: Space Physics*, *128*(11), e2023JA031486. https://doi.org/10.1029/2023JA031486

Nakashima, Y., Heki, K., Takeo, A., Cahyadi, M. N., Aditiya, A., & Yoshizawa, K. (2016). Atmospheric resonant oscillations by the 2014 eruption of the Kelud volcano, Indonesia, observed with the ionospheric total electron contents and seismic signals. *Earth and Planetary Science Letters*, *434*, 112–116. https://doi.org/10.1016/j.epsl.2015.11.029

Newhall, C. G., & Stephen, S. (1982). The volcanic explosivity index (VEI) an estimate of explosive magnitude for historical volcanism. *Journal of Geophysical Research: Space PhysicsOcean*, *87*, 1231–1238. https://doi.org/10.1029/JC087iC02p01231

Nina, A., & Čadež, V. (2013). Detection of acoustic-gravity waves in lower ionosphere by VLF radio waves. *Geophysical Research Letters*, *40*(18), 4803–4807. https://doi.org/10.1002/grl.50931

Nishida, K., Kobayashi, N., & Fukao, Y. (2014). Background Lamb waves in the Earth's atmosphere. *Geophysics Journal International*, *196*(1), 312–316. https://doi.org/10.1093/gji/ggt413

Ohya, H., Tsuchiya, F., Takamura, T., Shinagawa, H., Takahashi, Y., & Chen, A. B. (2024). Lower ionospheric resonance caused by Pekeris wave induced by 2022 Tonga volcanic eruption. *Scientific Reports*, *14*(1), 15659. https://doi.org/10.1038/s41598-024-65929-x

Pasko, V. P., Inan, U. S., & Bell, T. F. (1997). Sprites as evidence of vertical gravity wave structures above mesoscale thunderstorms. *Geophysical Research Letters*, *24*(14), 1735–1738. https://doi.org/10.1029/97GL01607

Poli, P., & Shapiro, N. M. (2022). Rapid characterization of large volcanic eruptions: Measuring the impulse of the Hunga Tonga Ha'apai explosion from teleseismic waves. *Geophysical Research Letters*, *49*(8), e2022GL098123. https://doi.org/10.1029/2022GL098123

Pradipta, R., Carter, B. A., Currie, J. L., Choy, S., Wilkinson, P., Maher, P., & Marshall, R. (2023). On the propagation of traveling ionospheric disturbances from the Hunga Tonga-Hunga Ha'apai volcano eruption and their possible connection with tsunami waves. *Geophysical Research Letters*, *50*(6), e2022GL101925. https://doi.org/10.1029/2022GL101925

Ravanelli, M., Astafyeva, E., Munaibari, E., Rolland, L., & Mikesell, T. D. (2023). Ocean-ionosphere disturbances due to the 15 January 2022 Hunga-Tonga Hunga-Ha'apai eruption. *Geophysical Research Letters*, *50*(10), e2022GL101465. https://doi.org/10.1029/2022GL101465

Richmond, A. D. (1978). Gravity-wave generation, propagation, and dissipation in thermosphere. *Journal of Geophysical Research*, *83*(A9), 4131–4145. https://doi.org/10.1029/ja083ia09p04131

Rodger, C. J. (2003). Subionospheric VLF perturbations associated with lightning discharges. *Journal of Atmospheric and Solar-Terrestrial Physics*, *65*(5), 591–606. https://doi.org/10.1016/s1364-6826(02)00325-5

Rodger, C. J., Cho, M., Clilverd, M. A., & Rycroft, M. J. (2001). Lower ionospheric modification by lightning EMP: Simulation of the nighttime ionosphere over the United States. *Geophysical Research Letters*, *28*(2), 199–202. https://doi.org/10.1029/2000gl011951

Rozhnoi, A., Hayakawa, M., Solovieva, M., Hobara, Y., & Fedun, V. (2014). Ionospheric effects of the Mt. Kirishima volcanic eruption as seen from sub ionospheric VLF observations. *Journal of Atmospheric and Solar-Terrestrial Physics*, *107*, 54–59. https://doi.org/10.1016/j.jastp.2013.10.014

Salut, M. M., Abdullah, M., Graf, K. L., Cohen, M. B., Cotts, B. R. T., & Kumar, S. (2012). Long recovery VLF perturbations associated with lightning discharges. *Journal of Geophysical Research*, *117*(A8), A08311. https://doi.org/10.1029/2012JA017567

Salut, M. M., Cohen, M. B., Ali, M. A. M., Graf, K. L., Cotts, B. R. T. S., & Kumar, S. (2013). On the relationship between lightning peak current and early VLF perturbations. *Journal of Geophysical Research: Space Physics*, *118*(11), 7272–7282. https://doi.org/10.1002/2013JA019087

Sentman, D. D., Wescott, E. M., Picard, R. H., Winick, J. R., Stenbaek-Nielsen, H. C., Dewan, E. M., et al. (2003). Simultaneous observations of mesospheric gravity waves and sprites generated by a midwestern thunderstorm. *Journal of Atmospheric and Solar-Terrestrial Physics*, *65*(5), 537–550. https://doi.org/10.1016/s1364-6826(02)00328-0

Solovieva, M. S., Padokhin, A. M., & Shalimov, S. L. (2022). Mega-eruption of the Hunga volcano on January 15, 2022: Detection of ionospheric perturbations by VLF and GNSS radio sounding. *JETP Letters*, *116*(11), 846–851. https://doi.org/10.1134/S0021364022602196

Solovieva, M. S., & Shalimov, S. L. (2022). Disturbances in the lower ionosphere after the eruption of the Hunga-Tonga-Hunga-Ha'apai volcano on January 15, 2022, recorded by the subionospheric VLF radio signals. *Doklady Earth Sciences*, *507*(2), 1080–1084. https://doi.org/10.1134/S1028334X22600840

Themens, D. R., Watson, C., Žagar, N., Vasylkevych, S., Elvidge, S., McCaffrey, A., et al. (2022). Global propagation of ionospheric disturbances associated with the 2022 Tonga volcanic eruption. *Geophysical Research Letters*, *49*(7), e2022GL098158. https://doi.org/10.1029/2022GL098158

Thomson, N. R., Clilverd, M. A., Brundell, J. B., & Rodger, C. J. (2021). Quiet night arctic ionospheric D region characteristics. *Journal of Geophysical Research: Space Physics*, *126*(4), e2020JA029043. https://doi.org/10.1029/2020ja029043

Thomson, N. R., Clilverd, M. A., & Rodger, C. J. (2014). Low-latitude ionospheric D region dependence on solar zenith angle. *Journal of Geophysical Research: Space Physics*, *119*(8), 6865–6875. https://doi.org/10.1002/2014ja020299

Thomson, N. R., Rodger, C. J., & Clilverd, M. A. (2005). Large solar flares and their ionospheric D region enhancements. *Journal of Geophysical Research*, *110*(A6), A06306. https://doi.org/10.1029/2005ja011008

Thomson, N. R., Rodger, C. J., & Dowden, R. L. (2004). Ionosphere gives size of greatest solar flares. *Geophysical Research Letters*, *31*, L06803. https://doi.org/10.1029/2003GL019345

Todoroki, Y., Maekawa, S., Yamauchi, T., Horie, T., & Hayakawa, M. (2007). Solar flare induced D region perturbation in the ionosphere, as revealed from a short-distance VLF propagation path. *Geophysical Research Letters*, *34*(3), L03103. https://doi.org/10.1029/2006GL028087

Vadas, S. L., Figueiredo, C., Becker, E., Huba, J. D., Themens, D. R., Hindley, N. P., et al. (2023). Traveling ionospheric disturbances induced by the secondary gravity waves from the Tonga eruption on 15 January 2022: Modeling with MESORAC-HIAMCMSAMI3 and comparison with GPS/TEC and ionosonde data. *Journal of Geophysical Research: Space Physics*, *128*(6), e2023JA031408. https://doi.org/10.1029/2023JA031408

Van Eaton, A. R., Lapierre, J., Behnke, S. A., Vagasky, C., Schultz, C. J., Pavolonis, M., et al. (2023). Lightning rings and gravity waves: Insights into the giant eruption plume from Tonga's Hunga Volcano on 15 January 2022. *Geophysical Research Letters*, *50*(12), e2022GL102341. https://doi.org/10.1029/2022GL102341

Vergoz, J., Hupe, P., Listowski, C., Le Pichon, A., Garcés, M., Marchetti, E., et al. (2022). Observations of infrasound and acoustic-gravity waves produced by the January 2022 volcanic eruption of Hunga, Tonga: A global analysis. *Earth and Planetary Science Letters*, *591*, 117639. https://doi.org/10.1016/j.epsl.2022.117639

Wait, J. R., & Spies, K. P. (1964). *Characteristics of the earth-ionosphere waveguide for VLF radio waves* Tech. Note 300. Nat. Burr. of Stand.

Wright, C. J., Hindley, N. P., Alexander, M. J., Barlow, M., Hoffmann, L., Mitchell, C. N., et al. (2022). Surface-to-space atmospheric waves from Hunga Tonga-Hunga Ha'apai eruption. *Nature*, *609*(7928), 741–746. https://doi.org/10.1038/s41586-022-05012-5

Wu, H., Lu, X., Wang, W., & Liu, H.-L. (2023). Simulation of the propagation and effects of gravity waves generated by Tonga volcano eruption in the thermosphere and ionosphere using nested-grid TIEGCM. *Journal of Geophysical Research: Space Physics*, *128*(4), e2023JA031354. https://doi.org/10.1029/2023JA031354

Xu, W., Feng, J., Gu, X., Ni, B., Wang, S., Cheng, W., et al. (2024). Periodic oscillation of VLF transmitter signals measured in low and middle latitude regions. *Journal of Geophysical Research: Atmospheres*, *129*(10), e2023JD040225. https://doi.org/10.1029/2023JD040225

Yuen, D. A., Melissa, A. S., Frank, J. S., Yingcai, Z., Hao, H., Stephen, R. M., et al. (2022). Under the surface: Pressure-induced planetary-scale waves, volcanic lightning, and gaseous clouds caused by the submarine eruption of Hunga Tonga-Hunga Ha'apai volcano. *Earthquake Research Advances*, *2*(3), 100134. https://doi.org/10.1016/j.eqrea.2022.100134

Zhang, S. R., Vierinen, J., Aa, E., Goncharenko, L. P., Erickson, P. J., Rideout, W., et al. (2022). Tonga volcanic eruption induced global propagation of ionospheric disturbances via Lamb waves. *Frontiers in Astronomy and Space Sciences*, *9*, 871275. https://doi.org/10.3389/fspas.2022.871275